Article

The Multiband over Spatial Division Multiplexing Sliceable Transceiver for Future Optical Networks

Laia Nadal *, Mumtaz Ali, Francisco Javier Vílchez, Josep Maria Fàbrega and Michela Svaluto Moreolo

Centre Tecnològic de Telecomunicacions de Catalunya (CTTC/CERCA), Parc Mediterrani de la Tecnologia—Building B4, Av. Carl Friedrich Gauss 7, 08860 Castelldefels, Spain; mali@cttc.es (M.A.); javier.vilchez@cttc.es (F.J.V.); jmfabrega@cttc.es (J.M.F.); michela.svaluto@cttc.es (M.S.M.)
* Correspondence: laia.nadal@cttc.es; Tel.: +34-93-645-29-00

Abstract: In the last 15 years, global data traffic has been doubling approximately every 2–3 years, and there is a strong indication that this pattern will persist. Hence, also driven by the emergence of new applications and services expected within the 6G era, new transmission systems and technologies should be investigated to enhance network capacity and achieve increased bandwidth, improved spectral efficiency, and greater flexibility to effectively accommodate all the expected data traffic. In this paper, an innovative transmission solution based on multiband (MB) over spatial division multiplexing (SDM) sliceable bandwidth/bitrate variable transceiver (S-BVT) is implemented and assessed in relation to the provision of sustainable capacity scaling. MB transmission (S+C+L) over 25.4 km of 19-cores multicore fibre (MCF) is experimentally assessed and demonstrated achieving an aggregated capacity of 119.1 Gb/s at 4.62×10^{-3} bit error rate (BER). The proposed modular sliceable transceiver architecture arises as a suitable option towards achieving 500 Tb/s per fibre transmission, by further enabling more slices covering all the available S+C+L spectra and the 19 cores of the MCF.

Keywords: adaptive loading; spatial division multiplexing; multiband transmission; sliceable transceiver

1. Introduction

Global data traffic has experienced significant growth in recent years, and it is expected to continue increasing primarily driven by the emergence of groundbreaking 6G applications and services, such as augmented reality, holographic communications, and even more sophisticated AI applications, which will require stringent requirements in terms of data rate/bandwidth and latency having an impact in the evolution of optical networks [1,2]. This exponential growth will imply a change in terms of volume and distribution of traffic in the network, highlighting the importance of flexible, robust, scalable, reliable, and high-capacity optical networks [3]. According to [1], in the aggregation metro segment, the flow capacities from access nodes directed towards additional nodes, particularly regional nodes, are foreseen to escalate to a maximum of 2 Tb/s in the medium term and an impressive 8 Tb/s in the long term. According to the estimations derived from traffic analysis of [1], regional and national nodes should efficiently manage the aggregated traffic, ranging from a few Tb/s in the short term, ten Tb/s in the medium term, and potentially reaching up to a hundred Tb/s in the long term. This underscores the need for robust and scalable infrastructure to accommodate the increasing demands on network resources over various time horizons from the access to the backbone network segments [4].

The landscape of 6G networks will also see significant enhancements in the wireless segment [5]. This includes more efficient wireless links that complement the wired infrastructure, providing seamless communication with final user devices enabling optical/wireless convergence [6,7]. The wireless segment for 6G is currently receiving high attention, and novel technologies such as THz, millilitre wave and visible light communications, integrated and free-space optics or power-over-fibre deployment as well as the

use and adoption of machine learning techniques, softwarization and massive multiple-input multiple-output signalling are under active investigation to provide additional features [7–14]. Notably, there is a focus on incorporating high-accuracy positioning, imaging and sensing capabilities, which are expected to play an important role for enabling services for all verticals within 6G networks.

The integration/convergence of both wired and wireless technologies is essential to meet the diverse and demanding requirements of 6G applications and support the incoming traffic increase [15]. The combination of high-capacity optical networks and advanced wireless links is crucial for ensuring the delivery of low-latency, high-throughput, and reliable connectivity. Moreover, as part of the evolution towards 6G, networks are anticipated to become more energy-efficient, contributing to the reduction in carbon footprints and aligning with global sustainability goals [16].

In this context, key advanced technologies including multiband (MB) and spatial division multiplexing (SDM) have been recently investigated for evolving current optical networks towards enabling the expected network capacity scaling. MB technology enables the utilization of additional bands beyond C-band, such as E-, S-, L-, O- and U-bands, in order to increase the available bandwidth of the fibre and optical spectrum resources [17]. This not only allows for the simultaneous transmission of data across various frequency bands, but also enhances the network's resilience and flexibility. Additionally, SDM enables to further enhance overall network capacity and scalability by exploiting multiple spatial channels, which can be based on a bundle of standard single-mode fibres (SSMFs) or even speciality fibres such as multicore fibres (MCFs) and few mode fibres (FMFs) [18,19]. By exploiting spatial diversity, SDM provides an advance in network capacity, enabling optical networks to accommodate an ever-expanding volume of data traffic. Together, MB and SDM technologies are capable of addressing the scalability challenges presented by 6G applications and services [20,21]. Specifically, the convergence of these two advanced technologies is anticipated to shape the landscape of optical networks in the 6G era by achieving:

(i) Enhanced bandwidth and spectral efficiency: MB enables to maximize the spectral resources, allowing for efficient data transmission across a wide range of frequencies/bands, while SDM exploits the spatial dimension such as cores/modes, dramatically increasing the network's capacity.

(ii) Enhanced network resilience and flexibility: by transmitting data simultaneously across various bands the systems will be more adaptable to dynamic network conditions. Additionally, the spatial diversity will also contribute to the resilience of optical networks. In the event of a failure in one spatial channel, the network can dynamically redistribute resources to maintain service continuity. Together, the convergence of MB and SDM technologies provides a comprehensive approach to fortifying optical networks against disruptions, ensuring robustness and adaptability.

(iii) Higher network scalability: Multiband over spatial division multiplexing (MBoSDM) technology addresses scalability challenges by efficiently utilizing available bandwidth across diverse bands and exploiting spatial diversity to increase network capacity. The combined effect of MB and SDM technologies is particularly relevant to meet the scalability demands and accommodate the ever-expanding volume of data traffic expected from the diverse range of applications and services anticipated in the 6G era.

Therefore, MBoSDM implies a transformation towards achieving unparalleled levels of efficiency, flexibility, and scalability in the 6G era harnessing the strengths of both technologies to address the evolving demands of data-intensive applications and services for the long-term period adoption within optical networks.

On this regard, the adoption of advanced transceiver architectures which can exploit MB and SDM technologies is fundamental in order to take advantage of the full potential of the networks. MB(oSDM) sliceable bandwidth/bitrate variable transceivers (S-BVTs) are proposed as an interesting transceiver option, based on a modular and scalable approach that can create a MB high-capacity flow that can be transmitted over different spatial

channels [22]. On the one hand, thanks to the transceiver modularity different building blocks can be enabled and disabled according to the network needs and traffic demand, enhancing network efficiency and flexibility. Specifically, this will allow network operators to dynamically allocate and adjust bandwidth and resources on-the-fly as needed. This flexibility maximizes the efficient use of available bandwidth, distributed to match the actual demand, reducing resource wastage and enhancing network performance. With the provision of transceiver scalability, additional slices/bandwidth can be added as necessary, ensuring the network can keep up with increasing demand. By enabling more dynamic and flexible network operation, sliceable transceivers can contribute to better network resilience. In the event of a failure in one slice, resources can be quickly redistributed to maintain service continuity. Finally, the efficient bandwidth utilization and the ability to scale as needed together with the possibility to adopt photonic integration approaches, that MB(oSDM) S-BVTs can offer, can lead to reduced power consumption and a smaller carbon footprint [23,24].

This work focuses on the design, implementation and experimental assessment of a MB(oSDM) S-BVT enabling up to 3 slices/flows within the C-, L-, and S-bands. The proposed transceiver approach exploits MB and SDM technologies and arises as a key solution to enhance overall network flexibility, efficiency, programmability and scalability toward meeting the stringent 6G capacity/bandwidth targets. In particular, Section 2 provides an overview of MB and SDM technologies. Then, Section 3 presents the MB(oSDM) S-BVT main architecture and key building blocks. Section 4 includes a numerical analysis of the optical signal crosstalk (XT) to evaluate the impact in different bands, such as O-, E-, S-, C-, L-, and U-bands. Then, the proof-of-concept of the proposed transceiver is explained in Section 5. The experimental assessment is performed in Section 6, where MB and MBoSDM transmission systems are evaluated. Additionally, in-band and out-band XT evaluation is also performed. Finally, in Section 7 the conclusions are drawn.

2. Enabling 6G Technologies

2.1. Multiband Technology

MB technology enables to significantly enhance the capacity of optical networks by simultaneously transmitting data in multiple frequency bands [25]. In particular, MB enables to expand the bandwidth of conventional standard single-mode fibres (SSMFs) by considering additional bands beyond C-band such as O-, E-, S-, C-, L-, and U-bands. This translates to an available optical bandwidth of 51.88 THz [26]. MB can provide cost-effective upgrades of optical networks by maximizing the utilization of already existing fibre infrastructure. The need for extensive new fibres can effectively be postponed while optimizing the return on investment. On the other hand, due to the frequency varying fibre characteristics (i.e., in terms of fibre attenuation/loss, chromatic dispersion (CD) and effective area), different performance is exhibited when transmitting in the different bands. This enables specific classes of applications and services with different requirements to be allocated accordingly within the differently performing bands. An optimal and dynamic resource allocation of the different frequency bands can be considered according to the varying network condition and traffic demands. However, MB transmission presents some challenges that should be considered. Specifically, the influence of stimulated Raman scattering (SRS) leads to a power transfer between wavelengths with a 100 nm spacing, as a result of the interplay of wavelength division multiplexing (WDM) channels across the various bands [17,27]. Additionally, the best technology option for amplification, filtering, modulation, and detection should be used according to the band of interest [28]. For example, regarding amplification, praseodymium-doped fibre amplifier (PDFA), neodymium DFA (NDFA), thulium DFA (TDFA), and erbium DFA (EDFA) could be considered for the O-band, E-band, S-band, and C+L-bands, respectively, [29]. Alternative solutions based on bismuth DFA, Raman amplifiers, or semiconductor optical amplifiers (SOA) can also be exploited [30]. All this poses new considerations and requirements in the design and implementation of novel MB transmission systems.

2.2. Spatial Division Multiplexing Technology

SDM technology encompasses diverse options, ranging from the deployment of bundled SSMFs to the utilization of speciality fibres such as few-mode, and multi-core fibres among others [31–33]. The deployment of new speciality fibres will require to establish a new transmission ecosystem and infrastructure translating to high CAPEX efforts. Hence, in the short/medium term, SDM could be exploited considering bundle of fibres in order to reach the high-capacity targets that 6G will pose, postponing other SDM solutions based on different fibre types for the long-term. These fibre technologies collectively open up the exciting potential for a substantial surge in the spatial–channel density within optical fibres, transcending the limitations of today's single-mode fibre solutions. The use of speciality fibres in the long-term will provide a more efficient and versatile approach to SDM, offering:

(i)　Enhanced spatial–channel density by supporting multiple channels within a single fibre.
(ii)　Reduced crosstalk due to speciality fibres are designed to minimize optical signal crosstalk between channels.
(iii)　Simplified network architecture by consolidating multiple channels into a single fibre.
(iv)　Improved spectral efficiency by allowing for the transmission of more information within the available bandwidth.
(v)　Lower latency due to the availability of more direct and efficient paths for data transmission, enhancing the overall performance of the network.
(vi)　Future-proofing providing high-scalability and efficiency for accommodating increasing demands.

Among the different highlighted speciality fibres, few-mode fibres, where a single, larger-area core accommodates multiple modes each propagating distinct information, presents some limitations. Specifically, modal dispersion, modal interference and high differential mode group delay can appear and limit the performance when co-propagating several modes [19,34]. MCFs, characterized by its multiple cores enveloped within a common cladding, can offer promising capacity upgrades in an efficient way [35]. However, optical signal XT, which can appear between cores, must be addressed and mitigated as part of the system's design and implementation [18,36,37]. To ensure the optimal performance of SDM technology, it is essential to align the transmission approach closely with the specific fibre design chosen for the application. In this paper, we will focus on MCF transmission, which seems to be one of the most efficient way to realize SDM, as a promising long-term solution that combined with MB technology can achieve the 6G stringent targets/requirements.

3. MB(oSDM) S-BVT Architecture and Definition

The proposed MB(oSDM) S-BVT architecture is depicted in Figure 1 and it is based on multiple bandwidth/bitrate variable transceivers (BVTs) that can be enabled/disabled based on traffic demands, following a modular and adaptable "pay-as-you-grow" framework. The envisioned architecture also facilitates MB point-to-point (PtP) and point-to-multipoint (PtMP) connectivity, by incorporating several BVTs designed to operate across various transmission bands, such as C-, L-, S-, O-, U-, and E-bands, as depicted in Figure 1. PtMP operation is achieved by the transceiver architecture's ability to manage multiple BVTs concurrently, enabling multiple network destinations or end-points to be served with a single S-BVT. This capability is especially valuable in scenarios where diverse and evolving communication requirements exist among various network destinations, including variations in path length and data rate requirements [38,39]. Whether addressing varying transmission distances or accommodating different data rate requirements, the transceiver architecture seamlessly adapts to these diverse needs. This flexibility is key in scenarios where a central node needs to communicate with multiple remote locations, each characterized by unique communication parameters. In this context, the advantage of utilizing a single MB(oSDM) S-BVT for P2MP operations lies in its ability to streamline network

infrastructure, reduce complexity, and enhance operational efficiency. Rather than deploying multiple transceivers to address individual communication links, the S-BVT optimizes resource utilization by managing multiple connections with a single, adaptable and programmable device. This not only simplifies the network architecture but also contributes to cost-effectiveness and ease of maintenance. Thanks to its scalable and modular architecture, it can easily accommodate the integration of new features and capabilities, thereby extending the useful lifespan of the equipment. At the digital signal processing (DSP) transmitter side of each BVT, adaptive loading based on orthogonal frequency division multiplexing (OFDM) is implemented, increasing the overall transceiver flexibility. Several operations are performed to generate the OFDM signals, such as data parallelization and mapping, insertion of training symbols (TS), implementation of the inverse fast Fourier transform, insertion of cyclic prefix (CP), serialization, and radio frequency (RF) up-conversion.
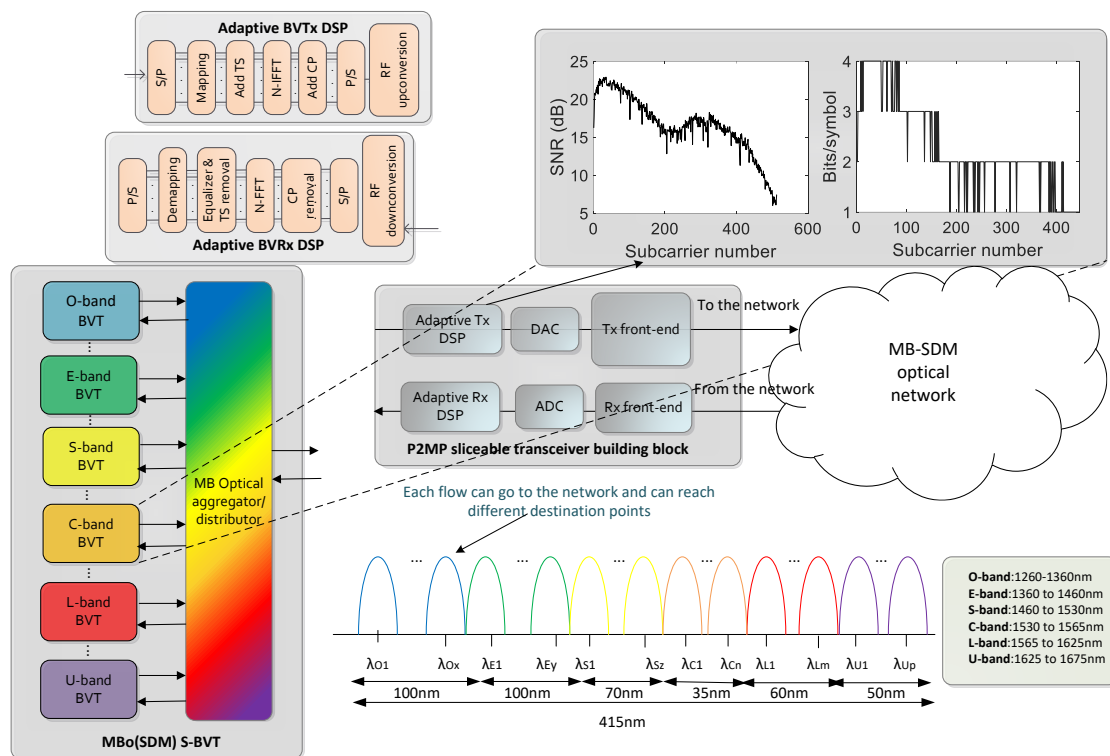

Figure 1. MB(oSDM) S−BVT architecture.

The implementation of bit and power loading (BPL) algorithms enable to dynamically adjust the power values and modulation format of each ODFM subcarrier to the specific profile of the channel, as depicted in Figure 1 [22]. This not only enhances the versatility of the transceiver, but also contributes to enhancing its overall performance. In the inset of Figure 1, it can be seen an example of the BPL operation, considering a C-band BVT based on intensity modulation (IM) and direct detection (DD) in a back-to-back (B2B) configuration, which assigns high modulation formats to the subcarriers that present highest performance/SNR. After DSP, digital-to-analogue conversion by means of a digital-to-analogue converter (DAC) is performed to generate an analogue OFDM signal. Different configurations can be adopted at the transmitter front-end of each MB S-BVT building block for modulation of the MB OFDM signals, such as IM, amplitude modulation or even IQ modulation [40]. Additionally, either external modulation (i.e., adopting Mach–Zehnder modulators—MZMs—and tuneable laser sources—TLSes) or direct modulation (i.e., using vertical cavity surface emitting lasers–VCSELs) can be adopted, trading-off performance versus cost/power consumption [22,41,42]. Finally, the different contributions are aggregated/distributed by means of an optical aggregator/distributor capable to allow operation across all the considered bands. This device is a key element of the MB S-BVT

architecture, that can be based on programmable filters capable to aggregate/disaggregated different MB slices [43]. However, due to low level of maturity of this technology, alternative solutions based on static/non-reconfigurable band pass filters (BPFs) can be considered. The receiver of the proposed MB S-BVT can be based on different implementations, such as DD or coherent detection, trading-off performance versus complexity/cost [22,42]. Analogue-to-digital converters (ADC) are included in the transceiver architecture to digitize the OFDM analogue signal, to perform the receiver DSP operations. These include RF down-conversion, data parallelization, CP removal, fast Fourier transform implementation, equalization, symbol de-mapping, and serialization. The presented sliceable architecture will enable to dynamically allocate its available MB bandwidth into smaller, independently manageable contributions, that can also be transmitted through different fibre spatial channels (i.e., fibre cores, modes) enhancing overall flexibility, scalability, and providing an efficient utilization of the MB and spatial resources. Thanks to the transceiver modularity and sliceability the MB flow can be disaggregated in an intermediate network node to transmit different set of bands/sub-bands, corresponding to different users/slices, to different fibre cores and destinations. The available MB and spatial resources can be dynamically adjusted and reallocated as needed, and the different contribution of the MB S-BVT can be sliced to different users or applications based on their specific requirements. Hence, capacity and performance will be maximized, leveraging the spatial and frequency domains, while meeting the diverse needs of various users and services. On the top of that, the adoption and implementation of a software defined networking (SDN) control plane and the corresponding SDN agents will be crucial to successfully adapt and configure the proposed transceiver solution [40].

4. Numerical XT Evaluation

MCF transmission arises as a promising SDM technology that can provide increased capacity, efficient use of space, high scalability, simplified network architecture, redundancy, reliability and energy efficiency, by the enabling of data transmission through different cores within the same optical fibre. However, XT can occur when signals from one core interfere with signals in adjacent cores. This interference can significantly degrade signal quality and network performance, and presents a dependence with frequency/wavelength. Hence, a proper design and signal isolation techniques are necessary to mitigate this issue, to achieve low XT levels between neighbouring cores. One effective technique to reduce the XT levels in MCFs is to employ a refractive index trench in the fibre design. A refractive index trench is a modification in the refractive index profile of the optical fibre, by forcing a trench or a low-index region around each core to effectively isolate the cores from one another. This can be strategically used to minimize XT between adjacent cores, as the refractive index trench acts as a barrier between the cores, preventing the leakage of light from one core to the neighbouring cores and hence enhancing the overall signal quality and reliability.

The refractive index trenches can be a powerful tool for reducing XT in MCF, and their design and implementation require careful engineering and optimization. As an example, Figure 2 shows the trench-assisted core design of 19-cores 25.4 km MCF considered for the experimental assessment in Section 6. In this context, the mean XT value of a core can be approximated through evaluating a straightforward analytical formula [44]. In fact, the homogeneous core single mode 19-core MCF is designed to achieve XT values between neighbouring cores of −25 dB, at 1550 nm, for a length of 25.4 km and a bending diameter of 159 mm. Hence, the impact of XT in different transmission bands can be numerically evaluated, also including the structural parameters and specifications of the 19-cores MCF of L = 25.4 km considered for the experimental assessment in Section 6. Specifically, the XT can be approximated through the following equation:

$$XT_\mu \approx \frac{2k_{pq}^2 R_b}{\beta \Lambda} L, \tag{1}$$

where Λ is the core pitch ($\Lambda = 34$ μm), k_{pq} is the mode linear coupling coefficient between two neighbouring cores (defined in Equation (2)), $R_b = 7.95$ cm is the bending radius, and β is the propagation constant. The propagation constant is defined as: $\beta = (2\pi)/(\lambda n_{eff})$, being λ the wavelength of operation and n_{eff} the core effective refractive index. The mode linear coupling coefficient in trench-assisted structures can be calculated considering the following equation:

$$k_{pq} = \frac{\sqrt{\Gamma}\sqrt{\Delta_1}}{a_1} \frac{U_1^2}{V_1^3 K_1^2(W_1)} \sqrt{\frac{\pi a_1}{W_1 \Gamma}} \exp\left[-\frac{W_1\Gamma + 2(W_2 - W_1)w_{tr}}{a_1}\right] \tag{2}$$

From Equation (2) and considering the approximations and simplifications in [44],

$$\Gamma = \frac{W_1}{W_1 + (W_2 - W_1)w_{tr}/\Lambda} \tag{3}$$

With a relative refractive index difference of $m = |\Delta_2|/\Delta_1 = 2$, W_2 and $(W_2 - W_1)$ can be approximated as linear functions of V_1, being $V_1 = \frac{2\pi}{\lambda}a_1 n_1 \sqrt{(2\Delta_1)}$, according to [44]. Specifically, $W_2 = 1.750V_1 - 0.388$, $(W_2 - W_1) = 0.607V_1 + 0.608$, n_1 is the core refractive index ($n_1 = 1.45$), a_1 is the core radius and w_{tr} is the trench width, as shown in Figure 2. Finally, $K_1(W_1)$ is the modified Bessel function of the 2nd kind with 1st order and $U_1^2 = a_1^2(k^2 n_1^2 - \beta^2)$, being $k = 2\pi/\lambda$.
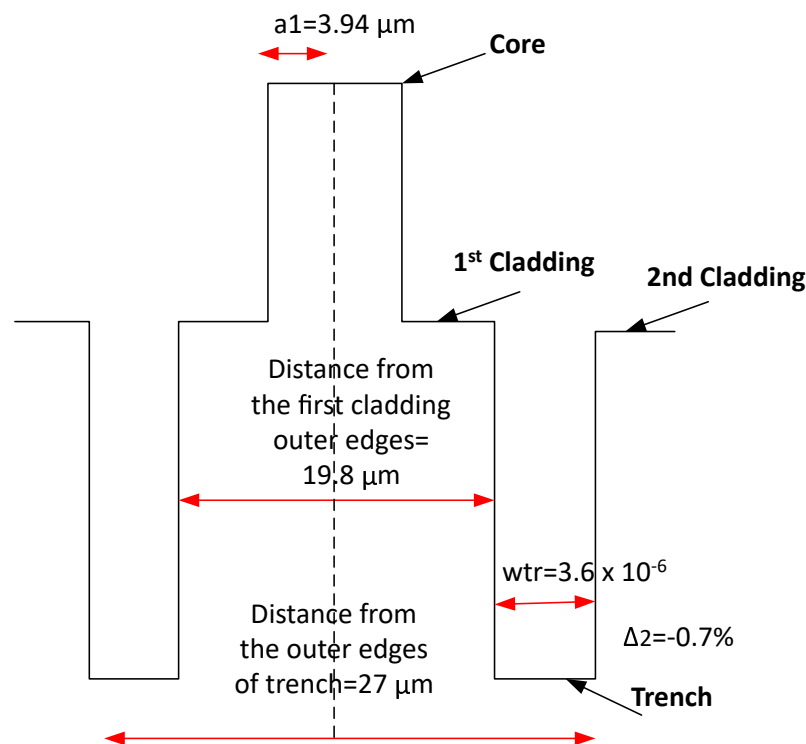

Figure 2. The trench−assisted core design of the 19−cores 25.4 km MCF considered for the experimental assessment in Section 6.

Following this analysis, the estimated XT per wavelength is depicted in Figure 3. A range from 1260 nm to 1675 nm—covering the whole of the O-, E-, S-, C-, L-, and U-bands [26]—has been taken into account. From the figure, it can be seen that the O-band is the spectral band less affected by the XT, presenting values below −50 dB, whereas within the C-band, the XT values range between −30 dB and −25 dB. In particular, at 1550.12 nm the XT value is −26.1 dB, which perfectly match the measured XT mean value of the MCF specifications of −25.5 dB. Finally, the U-band presents a higher XT degradation, presenting values higher than −20 dB. Figure 4 presents an evaluation of the XT considering different

MCF lengths up to 279.4 km, corresponding to 11 spans of 25.4 km. In this particular scenario, central wavelengths of the different analysed bands are considered to perform the XT analysis: specifically, 1310 nm (O-band), 1410 nm (E-band), 1495 nm (S-band), 1550 nm (C-band), 1600 nm (L-band), and 1650 nm (U-band). The achieved numerical results show an increase in the XT effect at the increase in the MCF length. As it is also seen in Figure 4, the U-band presents higher XT impact, showing values from −15 dB (after 25.4 km) up to −5 dB (after 279.4 km). After the maximum analysed MCF length of 279.4 km, −48 dB, −33.4 dB, −22.3 dB, −15.7 dB, and −10.1 dB are measured at O-, E-, S-, C-, and L-bands, respectively.
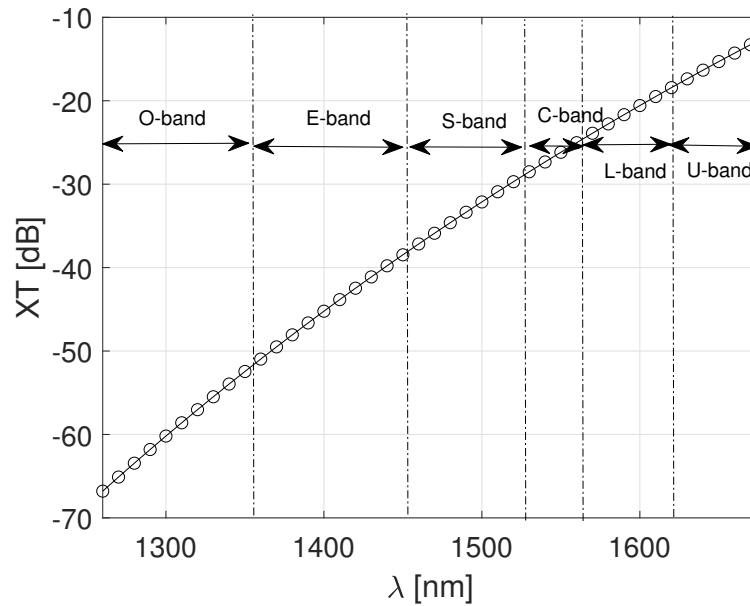

Figure 3. Estimated XT versus wavelength in a trench−assisted 19−cores MCF of 25.4 km.
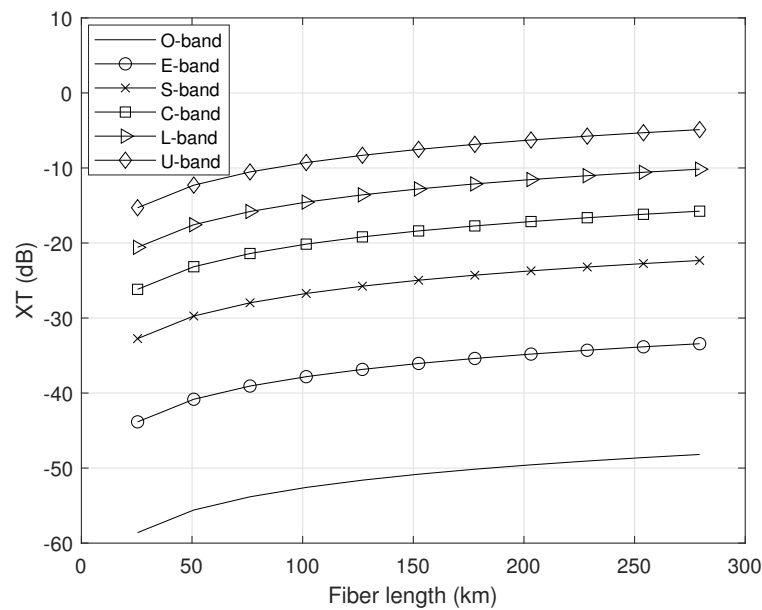

Figure 4. XT analysis over different MCF lengths and considering MB transmission in the O-, E-, S-, C-, L-, and U-bands.

5. Setup Implementation and Proof-of-Concept

For the proof-of-concept assessment of the MB(oSDM) S-BVT, 3 different slices working at the S-, C-, and L-bands are enabled, as depicted in Figure 5. Specifically, adaptive modu-

lation based on the Levin–Campello loading algorithm is performed at each transceiver building block, to flexibly adapt the modulation format and power value per subcarrier according to the channel profile [22]. After performing the different DSP operations described in Section 3, a high-speed DAC at 64 GSa/s is used to generate an OFDM electrical signal of 512 subcarriers and 20 GHz bandwidth. The transceiver front-end is based on external modulation and includes an array of lasers, that can be set up within the S-, C-, and L-bands, and MZMs working at the quadrature point. In particular, an electro-absorption modulated laser (EML) set to 1500 nm is used for the S-band contribution with 150 kHz linewidth. 2 TLSes at 1550.12 nm and 1600 nm are used for the C- and L-bands with linewidth values < 100 KHz and equal to 500 kHz, respectively. The output power of the three contributions are set to 10 dBm. A MB high-capacity flow is created by means of an optical aggregator, which includes single side band (SSB) filters and a BPF. SSB modulation is implemented within the C- and S-band slices, by including a wavelength selective switch (WSS) of 25 GHz bandwidth and a tuneable filter (TF) of 30 GHz bandwidth, respectively. This increases the resiliency against chromatic dispersion, enhancing overall performance. However, due to laboratory/setup limitations, the L-band contribution is not filtered and a DSB signal is aggregated with the other contributions. The transmitted MB high-capacity flow can be seen in Figure 6, as well as the detailed S-, C-, and L-band spectra.
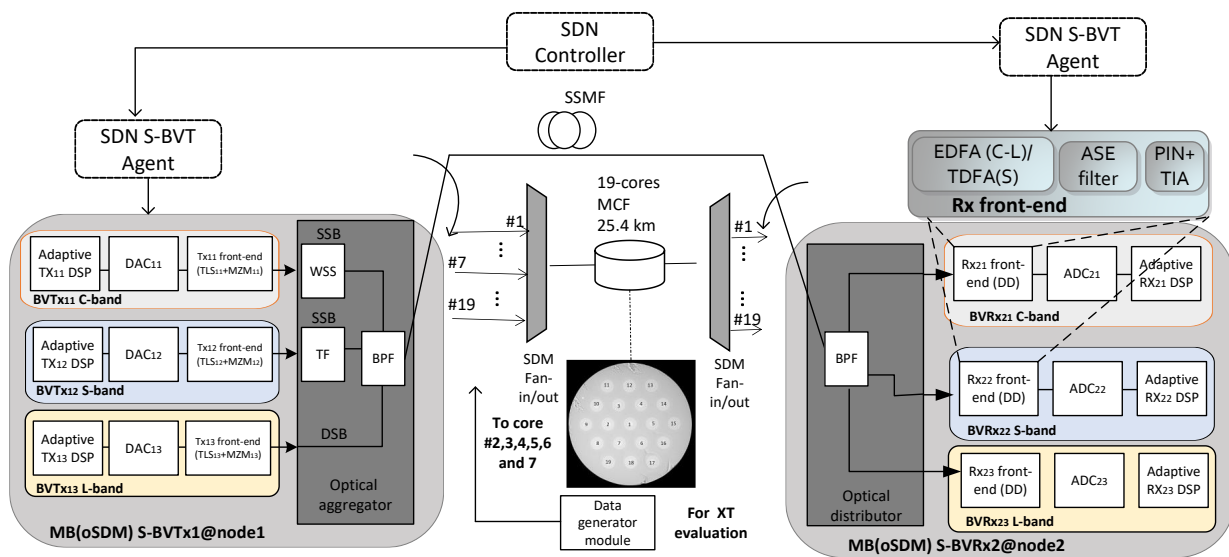

Figure 5. Experimental setup illustrating an S−BVTx at node 1 (S−BVTx1) and an S−BVRx at node 2 (S−BVRx2).

At the receiver side of the proposed MB(oSDM) S-BVT, an optical distributor is included, based on a BPF. The different slices are distributed to the corresponding bandwidth/bitrate variable receivers (BVRxs), adopting specific components/technology capable to operate in a particular band. Specifically, an EDFA (operating at automatic power control mode) and a WSS for amplified spontaneous emission (ASE) noise filtering (centred at 1550.12 nm and 50 GHz bandwidth) are used at the receiver front-end, for the C-band contribution. The S-band slice is amplified with a TDFA (operating at automatic current control mode) and filtered with a static filter, whereas an EDFA (operating at auto current control mode) and a static filter are considered at the L-band. All the contributions are photodetected with different PINs and ADC converted with an oscilloscope at 100 GSa/s. Additional DSP and performance parameters (summarized in Table 1) have been considered for the experimental assessment of Section 6.

Table 1. DSP and performance parameters.

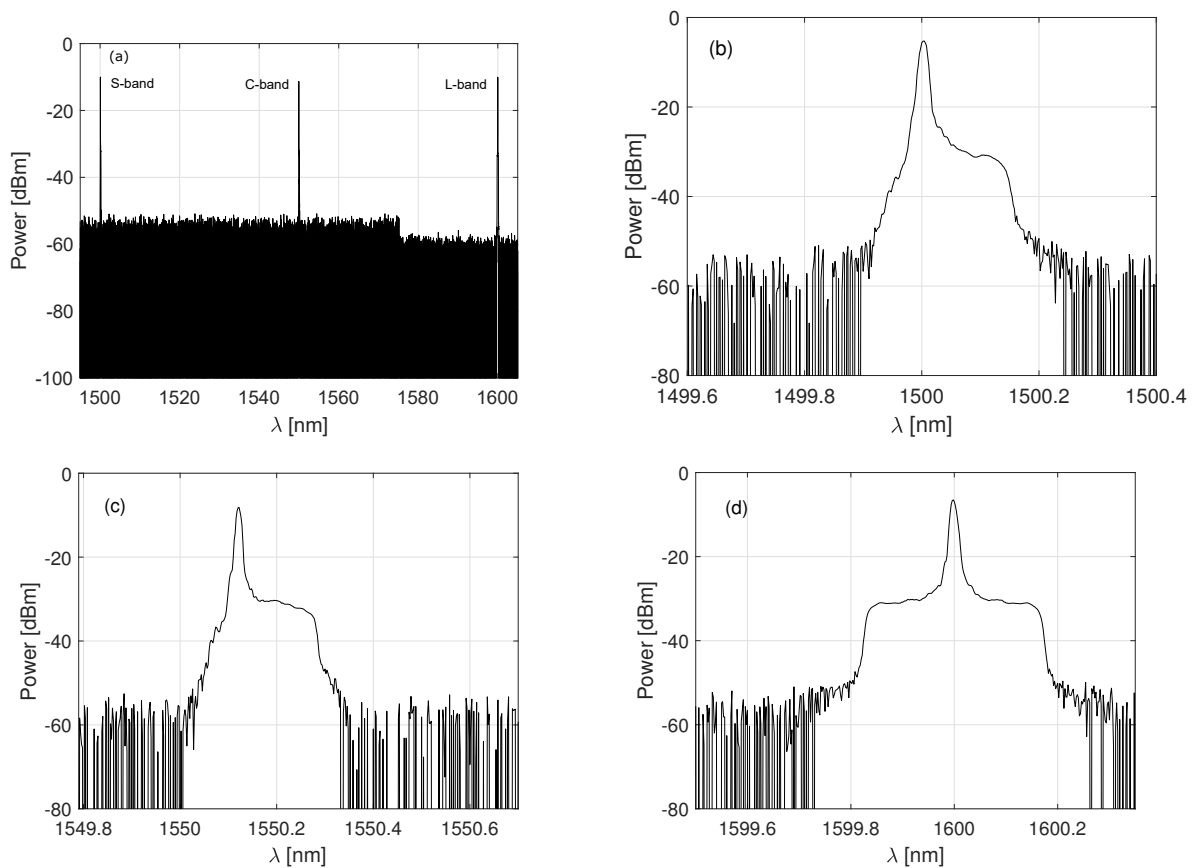| Parameter	Value
CP overhead	4%
TS overhead	1.9%
FEC overhead	7%
FEC type	HD-FEC
Target BER	4.62×10^{-3}

Figure 6. (**a**) Transmitted MB high−capacity flow after MB(oSDM) S−BVT optical aggregator; (**b**) S-band SSB; (**c**) C-band SSB; (**d**) L-band DSB-transmitted spectra.

6. Experimental Assessment

This section summarizes the main achieved results of the analysis and assessment of the proof-of-concept of the MB(oSDM) S-BVT. We have targeted two different scenarios/use cases to assess the different capabilities and operation modes of the proposed transceiver, for both MB and MBoSDM transmission. For MB transmission assessment, the generated MB (S+C+L) high-capacity flow is transmitted over different fibre spools of G.652D SSMF up to 75 km [45]. The SSMF, presents a CD coefficient of 17 ps/(nmkm) at 1550 nm and a mode field diameter (MFD) in the range of 8.6–9.2 μm at 1310 nm. In this particular scenario of assessing MB transmission, the data generator module of Figure 5 is not activated. Additionally, a 19-cores MCF of 25.4 km is considered to assess the MBoSDM transmission. The MCF has a MFD >7.88 μm, corresponding to the fibre core diameter. The MB signal (S+C+L) is transmitted over core #1, whereas the adjacent cores (# 2, 3, 4, 5, 6, and 7) are filled with alternative data signals generated to evaluate both the in-band and out-band XT, as it will be explained and detailed later in this section. The alternative data are created by enabling the data generator module of Figure 5 to fill the adjacent/neighbouring cores of the MCF with data to evaluate the XT effect. In the following experiments we consider

that each fibre core can support the transmission of all bands and each band can convey different user data.

6.1. MB Transmission Assessment

In a first use case, MB transmission is assessed considering the experimental setup described in Section 5. The signal–noise ratio (SNR) profiles in a B2B configuration are depicted in Figure 7. From the figure, it can be seen that the three slices, working in different bands, present similar performance in terms of SNR per subcarrier. Mainly, the degradation of the higher frequencies, corresponding to the higher subcarrier numbers, is due to the limited bandwidth of the DAC, which is around 13 GHz bandwidth. In particular, the electrical OFDM signal occupies 20 GHz bandwidth, corresponding to 512 subcarriers. Considering a SSMF path of 25 km length, the SNR profiles present different performance per each band, as seen in Figure 8d. The DSB L-band contribution is more affected by CD, showing two attenuation peaks within the signal bandwidth at around 11 GHz (subcarrier 281) and 19 GHz (subcarrier 488). This translates to a CD coefficient of 19.4 ps/(nmkm) at 1600 nm, according to Equation (4):

$$f_{CD}^n = \sqrt{\frac{c(2n-1)/2\lambda^2}{LD}}. \tag{4}$$

D is the dispersion coefficient parameter, c the speed of light and f_{CD}^n the n-th attenuation peak due to CD. The C- and L-band contributions are more resilient against CD, due to SSB modulation showing a flatter SNR profile. However, they present lower SNR values within the lower frequencies/subcarriers due to the setup implementation. In particular, different lasers, filter and amplification technology are used to set up the 3 BVTs conforming the MB S-BVT. BPL is applied to compensate the SNR degradation that specific subcarriers present in order to ensure the transmission at the target BER.
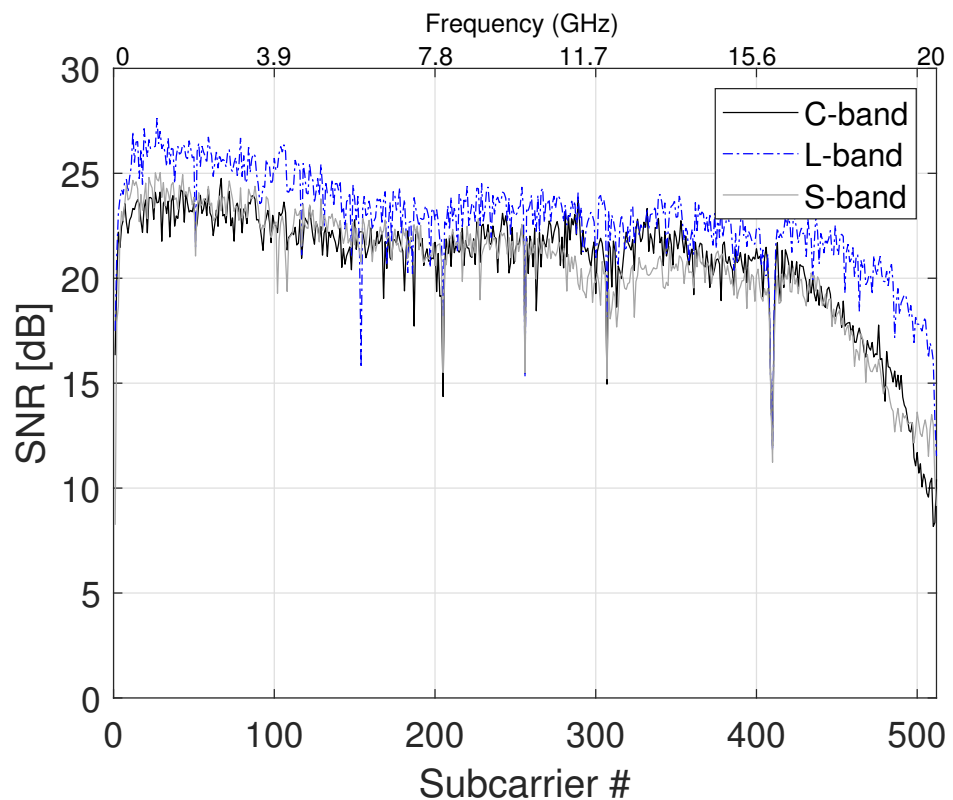

Figure 7. SNR profile of the S-, C-, and L-band contributions in B2B configuration.
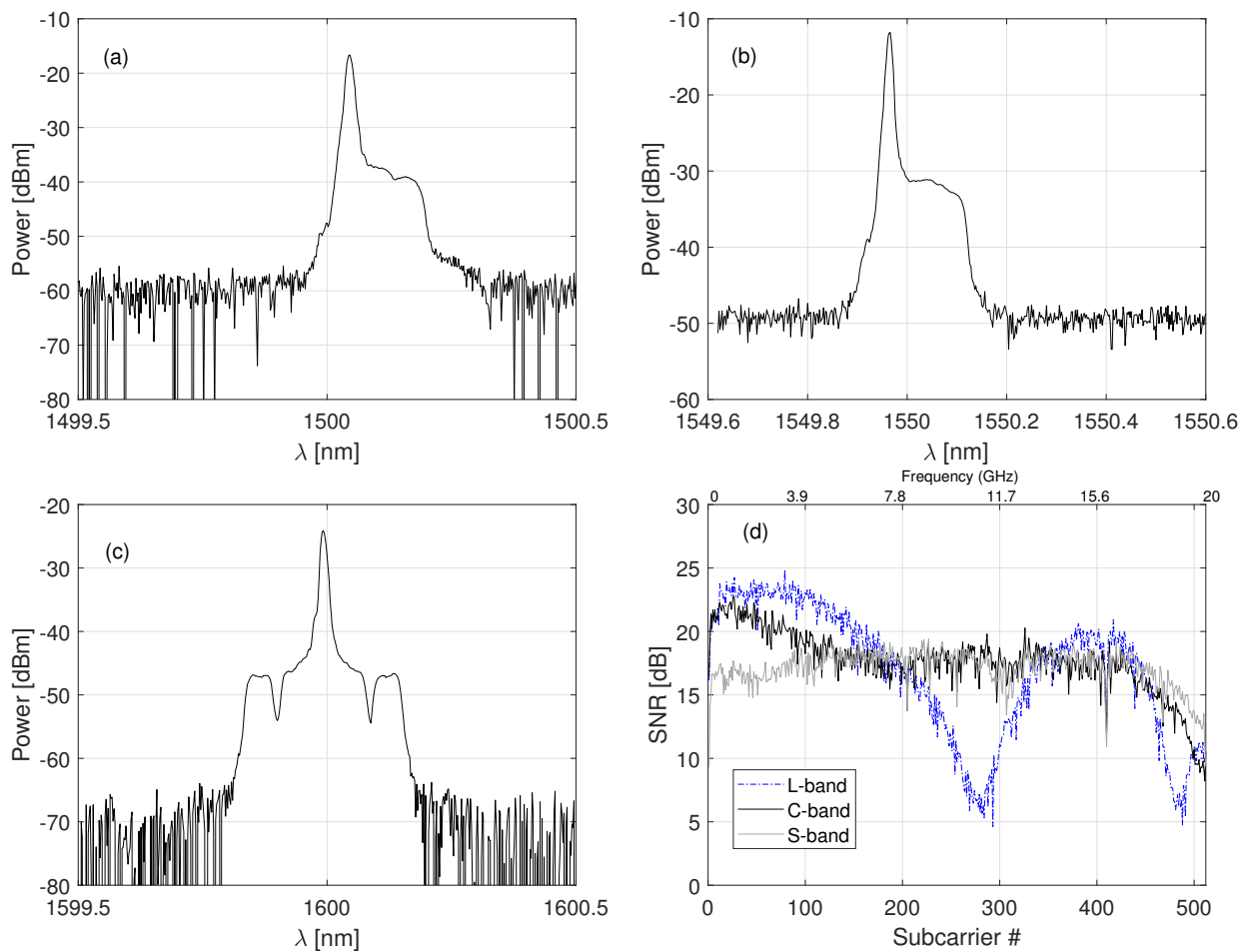
Figure 8. OSA captures after applying BPL and after 25 km of SSMF of the (**a**) S-band (**b**) C-band, and (**c**) L-band slices. (**d**) SNR profile of the S-, C-, and L-band contributions after 25 km of SSMF.

The received spectra after amplification and applying BPL are depicted in Figure 8. From the DSB L-band spectrum, depicted in Figure 8c, it could be seen that the implemented BPL algorithm has set to 0 the subcarriers with lower SNR. The SSB C-band and L-band spectra, in Figure 8a,b, show 5 dB power attenuation due to fibre transmission over a 25 km path in comparison with the B2B spectra of Figure 6. The achieved performance in terms of maximum data rate is depicted in Figure 9, for different SSMF lengths. In the B2B configuration, an aggregated capacity of 212 Gb/s is achieved ensuring the target BER. After 25 km SSMF, this data rate decreases to 134 Gb/s, and thanks to the implementation of BPL algorithms, the 3 contributions still present similar performance. After 50 km and 75 km path, the aggregated capacity decreases to 107 Gb/s and 73 Gb/s, respectively. Due to setup implementations, the L-band contributions can achieve higher OSNR values. However, the DSB transmission is more affected by CD. This effect can be seen in terms of achieved data rate in Figure 9, where the C-band contributions outperforms L-band contribution after transmission over the fibre with lower OSNR values.

Regarding the transceiver scalability, the modular architecture of the MB(oS-BVT) S-BVT enables the use of more slices in the different bands, in order to enable higher capacities. Specifically, by considering the full population of the analysed bands with 25 GHz (S+C) and 50 GHz (L-band) channel bandwidths, a total aggregated capacity of 47 Tb/s is envisioned in B2B configuration. This corresponds to 23 Tb/s for the S-band (350 channels), 12 Tb/s for the C-band (175 channels), and 12 Tb/s for the L-band (150 channels).
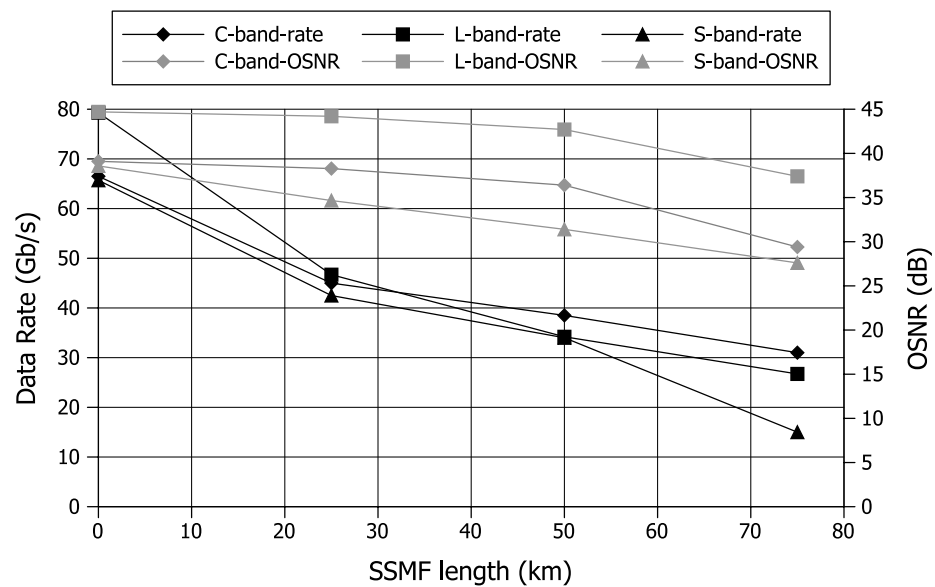
Figure 9. Achieved maximum data rate and OSNR per slice considering different fibre paths of up to 75 km length.

6.2. MBoSDM Transmission Assessment

A second experimental assessment is performed for the MBoSDM transmission, as a key scenario to provide the required capacity scaling expected in future networks. Hence, a 19-cores MCF of 25.4 km is considered in the setup of Figure 5 to evaluate the performance of the proposed MB(oSDM) S-BVT. The total optical power of the C-, L-, and S-bands optical signals launched into the MCF fibre, measured in the optical spectrum analyser (OSA), is −1.6 dBm. In this particular scenario, the estimated SNR profile per subcarrier is depicted in Figure 10a, showing the CD impact on the DSB L-band contribution. Specifically, the first attenuation peak due to CD appears at 10.9 GHz corresponding to a CD coefficient of 19.4 ps/(nmkm) at 1600 nm, according to Equation (4). Additionally, a degradation in terms of SNR is shown when comparing with the SSMF path of 25 km, depicted in Figure 8d. In fact, for this particular length the MCF presents higher attenuation values per core, of up to 10 dB (measured within the C-band), with respect to the 5 dB attenuation within the SSMF. A first assessment is performed without considering the XT. In this particular case, the achieved capacity per band after transmitting over the MCF is shown in Figure 10b. From the figure, it can be seen that the C-band contribution achieves the highest data rate of 44 Gb/s at the target BER and 36 dB optical signal noise ratio (OSNR). A capacity of 35.8 Gb/s (L-band) and 39.3 Gb/s (S-band) is obtained at 37.8 dB OSNR and 31.7 dB OSNR, respectively. In fact, when transmitting across the MCF, different performance per band is expected due to the wavelength dependence of fibre properties, such as effective area, CD and fibre attenuation/loss.

Thanks to the exploitation of SDM, spatial dimension can be also considered and new resources are available to further scale overall network capacity. A full population of the S+C+L-bands with a single core of the 19-cores MCF will envision data rates of 13.8 Tb/s for the S-band (350 channels), 7.7 Tb/s for the C-band (175 channels) and 5.5 Tb/s for the L-band (150 channels). Hence, considering S+C+L bands and the 19 cores, the aggregated capacity can scale up to 500 Tb/s (19*x*27 Tb/s).
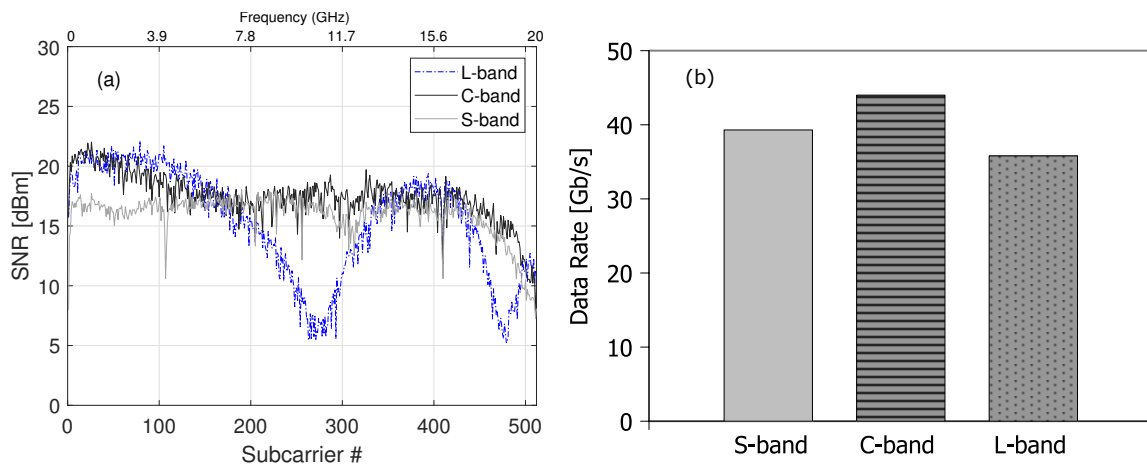
Figure 10. (**a**) SNR profile of the S-, C-, and L-band contributions and (**b**) achieved data rate per band after 19−cores MCF of 25.4 km.

Out-Band and In-Band XT Evaluation

Here, the out-band and in-band XT are evaluated using the data generation module of Figure 5, which feeds the adjacent cores (#2, 3, 4, 5, 6, and 7) of the MCF. In particular, for the out-band XT assessment, the data generation module consists of the S-band amplified contribution after the MCF. The S-band amplifier (TDFA-based) pump laser diode (LD) current is varied in steps of 100 mA up to a maximum value of 500 mA, to evaluate the impact of the out-band XT within the C-band and L-band. However, similar capacity of about 38 Gb/s is obtained in all the analysed cases, as the OSNR slightly varies around 34 dB. This translates to 6 Gb/s data rate decrease in comparison with the scenario that not considers XT, where 44 Gb/s was achieved at 35 dB OSNR. In the case of L-band, the same data rate of 35.8 Gb/s is achieved at the target BER, and 37.8 dB OSNR with and without out-band XT, as the selected S-band and L-band wavelengths are 100 nm separated.

Finally, the in-band XT within the C-band is evaluated. In this scenario, the data generation module of Figure 5 is based on a C-band broadband source (BS) and an EDFA. The power profile before and after amplification is shown in Figure 11. We have varied the output power of the EDFA in order to vary the impact of the in-band XT. As a result, the achieved data rate versus OSNR is depicted in Figure 12. From the figure, it can be seen that a maximum data rate of 44 Gb/s (point A) is achieved without XT at 35 dB OSNR and the target BER. The data rate of the C-band contribution decreases with the increasing of the in-band XT signal power down to 22 Gb/s (point B) at 23.6 dB OSNR. So, despite the MCF is designed to reduce the XT levels, when the signal power of the neighbouring/adjacent cores is very high, it can lead to XT issues and interfere with the signal of interest by inducing optical interference and unwanted coupling between the cores, degrading the overall performance and limiting the capacity, as seen in the results of Figure 12. This highlights the importance of managing signal power levels of the different cores, to minimize the in-band XT for reliable communication.

6.3. Complexity/Cost Analysis of the Proposed MB(oSDM) S-BVT

In this paper, we have proposed to implement a MB(oSDM) S-BVT based on IM and DD to target cost efficiency when comparing with alternative implementations based on coherent detection taking advantage of cost-effective optoelectronic subsystems and simplified DSP. According to [46], the adoption of DD technology, at the receiver side, instead of coherent detection reduces the S-BVT cost of about 25–35%. Additionally, a comparison of the cost of 2 × 50 Gb/s S-BVT based on DD and coherent solution at 100 Gb/s (4 × 25 Gb/s) is provided in [46], showing intrinsic cost savings when adopting a DD implementation. However, the proposed MB(oSDM) S-BVT, of Figure 1, has additional elements to consider in terms of cost analysis due to the exploitation of MB technology.

Hence, here we provide a cost analysis of the proposed transceiver solution based on external modulation and simple DD photodetection. For the cost analysis, we consider that the optical aggregator/distributor element of the MB(oSDM) S-BVT comprises WSSes shared among all the BVTs working in a specific band and BPFs to implement MB technology. Table 2, shows the number of components required to implement the proposed transceiver based on DD considering 3 transmission slices at different bands (S+C+L) at 50 Gb/s.
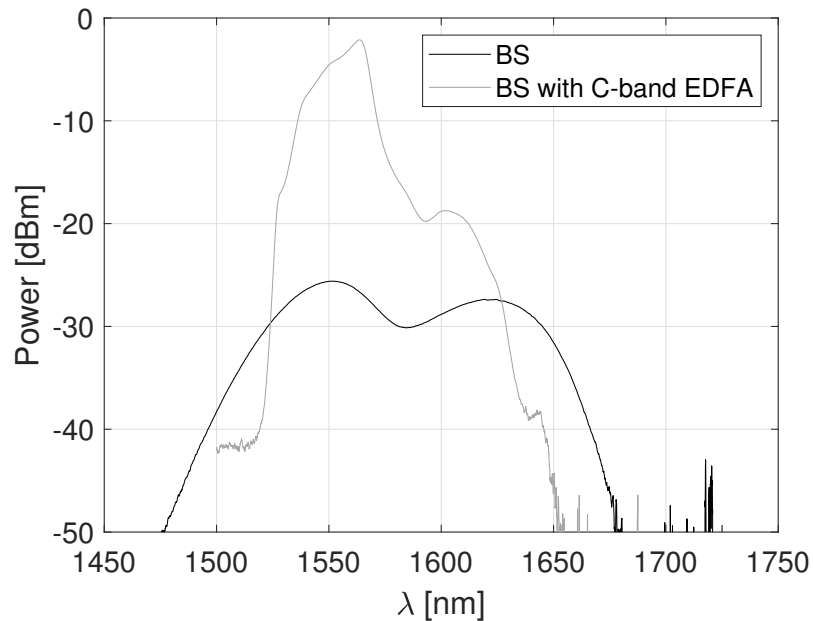

Figure 11. Power profile of the data filled in the neighbouring cores of the MCF to evaluate the XT. BS−broadband source; EDFA−erbium-doped fibre amplifier.
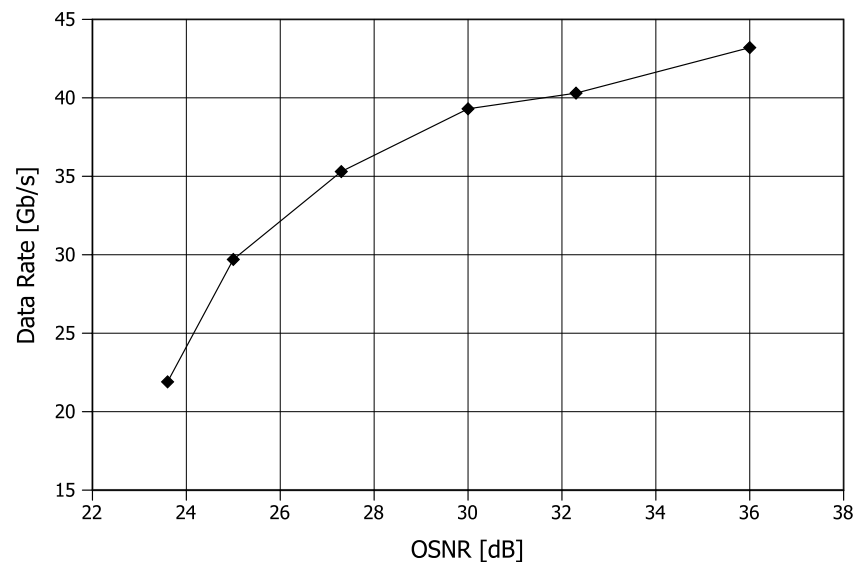

Figure 12. Maximum achieved data rate for the C-band contribution, considering in-band XT.

Thus, the unitary cost of a building block in the C-band of the proposed MB(oSDM) S-BVT based on DD is:

$$C_{BVT_{xC}} = C_{LS_C} + C_{MZM} + C_{driver} + \frac{C_{DAC}}{M} + \frac{C_{WSS_{TxC}}}{N} + \frac{C_{BPF}}{B} \qquad (5)$$

$$C_{BVR_{xC}} = C_{PD} + \frac{C_{ADC}}{M} + \frac{C_{WSS_{RxC}}}{N} + \frac{C_{BPF}}{B} \qquad (6)$$

M and N are the number of DAC/ADC and WSS ports, respectively, and B the number of BPF outputs, corresponding to the number of bands. We have considered that the WSS working in a particular band at the transmitter and receiver are the same. The unitary cost for the L-band and S-band building blocks will depend on the same individual parts/elements which include the LS, MZM, driver, DAC, WSS, PD, ADC, and BPF. However, the cost of specific components such as LS and WSS working in S- and L-bands are higher than the ones in the C-band due to the availability and maturity of the technology in the specified bands. As an example, the cost of the S-band LS (EML) used in the experiments is almost 5 times higher than the cost of the C-band LS (TLS), which both are from the same provider/manufacturer. Additionally considering similar WSS modules from the same provider, the cost of the WSS in the L-band can be increased by a factor of 1.3 when comparing with the C-band one. Hence, we consider α, β, γ, and ϵ scaling factors > 1 to define the relationship in terms of cost of the LS and WSS in the S- and L-band with the corresponding C-band elements, respectively. Taking into account all this, the total cost for the 150 Gb/s MB(oSDM) S-BVT (3 × 50 Gb/s) can be defined as:

$$
\begin{aligned}
C_{S-BVT} = {} & (1+\alpha+\beta) \times C_{LS_C} + 3 \times C_{MZM} + 3 \times C_{driver} + + 3 \times \frac{CDAC}{M} + \\
& + 3 \times \frac{CADC}{M} + 2 \times (1+\gamma+\epsilon) \times \frac{CWSS_C}{N} + 3 \times C_{PD} + 6 \times \frac{CBPF}{B}
\end{aligned}
\tag{7}
$$

According to Equations (5) and (6) and reference [46], the cost of the MB(oSDM) S-BVT, when only enabling the C-band, will slightly increase compared to a S-BVT that can not enable MB technology. Specifically, this increase is mapped with the cost term of using BPFs ($2 \times \frac{CBPF}{B}$), which are static filters using very cheap technology of the order of few hundred euros. The seemingly extra cost of deploying the MB(oSDM) S-BVT is justified by the substantial improvements it brings to the optical network's capabilities. In particular, the increased available spectral resources and the dynamic capacity scalability by enabling multiple slices in different bands beyond C-band. It is also worth to point out that due to the higher-cost of technology beyond C-band it will exist a trade-off between performance/capacity and cost. This trade-off introduces a strategic decision point that network planners and operators will carefully evaluate from a holistic network perspective before taking specific actions.

Table 2. Number of elements for a MB(oSDM) S-BVT with DD.

Component	MB(oSDM) S-BVT DD
MZM	3
Driver	3
DAC	3 ports
ADC	3 ports
(Laser source) LS_S	1
LS_C	1
LS_L	1
WSS_{TxS}	1 port
WSS_{TxC}	1 port
WSS_{TxL}	1 port
WSS_{RxS}	1 port
WSS_{RxC}	1 port
WSS_{RxL}	1 port
BPF_{Tx}	3 outputs
BPF_{Rx}	3 outputs
Photodetector (PD)	3

7. Conclusions and Future Directions

A modular and scalable MB(oSDM) S-BVT is proposed as a key element to provide suitable capacity scaling to meet the demands of future optical networks. A proof-of

concept of the proposed transceiver based on DD and adaptive OFDM, considering 3 slices working within the S-, C-, and L-bands, is experimentally assessed. MB and MBoSDM transmission is demonstrated over a SSMF path of 75 km and a 19-cores MCF of 25.4 km length. Aggregated capacities of 212 Gb/s and 119 Gb/s are achieved ensuring the target BER in a B2B configuration and after the 25.4 km MCF path, respectively. Thanks to the scalable transceiver architecture and the exploitation of MB and SDM technologies, 500 Tb/s per fibre transmission can be envisioned with the full population of the three analysed bands and the 19 cores of the MCF. The impact of XT in the transmission is numerically and experimentally evaluated, highlighting the importance of managing signal power levels feed into the different cores of the MCF system. Additionally, a complexity/cost analysis of the proposed transceiver solution has been included analysing the impact of enabling MB technology. The presented preliminary assessment of the proposed transceiver shows the benefits and advantages of MBoSDM as key strategy to be adopted in future optical networks towards supporting the expected traffic demand and stringent requirements. On this regard, the investigation of additional spectral bands beyond S+C+L bands and related transmission impairments will be crucial to analyse the capabilities of the technology/solution. Finally, the interaction and integration of the proposed transceiver in a MBoSDM network is also a challenge to be addressed to validate the full potential of the proposed approach.

Author Contributions: Conceptualization, L.N., J.M.F. and M.S.M.; methodology, L.N., J.M.F. and M.S.M.; software, L.N. and J.M.F.; validation, L.N., M.A. and F.J.V.; investigation, L.N., J.M.F. and M.S.M.; resources, L.N.; data curation, L.N.; writing—original draft preparation, L.N.; writing—review and editing, L.N., J.M.F., M.A., F.J.V. and M.S.M.; visualization, F.J.V.; supervision, L.N. All authors have read and agreed to the published version of the manuscript.

Data Availability Statement: Data sharing not applicable.

Conflicts of Interest: The authors declare no conflict of interest.

References

1. Ruiz, M.; Hernandez, J.A.; Quagliotti, M.; Hugues Salas, E.; Riccardi, E.; Rafel, A.; Velasco, L.; Gonzales De Dios, O. Network Traffic Analysis under Emerging Beyond-5G Scenarios for Multi-Band Optical Technology Adoption. *JOCN* **2023**, *15*, F36–F47. [CrossRef]
2. Winzer, P.J.; Neilson, D.T.; Chraplyvy, A.R. Fiber-optic transmission and networking: The previous 20 and the next 20 years. *Opt. Express* **2018**, *26*, 24190–24239. [CrossRef] [PubMed]
3. Lord, A.; Savory, S.J.; Tornatore, M.; Mitra, A. Flexible Technologies to Increase Optical Network Capacity. *Proc. IEEE* **2022**, *110*, 1714–1724. [CrossRef]
4. Fiorani, M.; Skubic, B.; Mårtensson, J.; Valcarenghi, L.; Castoldi, P.; Wosinska, L.; Monti, P. On the design of 5G transport networks. *Photon. Netw. Commun.* **2015**, *30*, 403–415. [CrossRef]
5. Pérez, G.O.; Hernández, J.A.; Larrabeiti, D. Fronthaul Network Modeling and Dimensioning Meeting Ultra-low Latency Requirements for 5G. *J. Opt. Comm. Netw.* **2018**, *10*, 573–581. [CrossRef]
6. Filgueiras, H.R.D.; Lima, E.S.; Cunha, M.S.B.; Lopes, C.H.D.S.; De Souza, L.C.; Borges, R.M.; Cerqueira, A. Wireless and Optical Convergent Access Technologies Toward 6G. *IEEE Access* **2023**, *11*, 9232–9259. [CrossRef]
7. Raddo, T.R.; Rommel, S.; Cimoli, B.; Vagionas, C.; Perez-Galacho, D.; Pikasis, E.; Tafur Monroy, I. Transition technologies towards 6G networks. *Wirel. Commun. Netw.* **2021**, *2021*, 100. [CrossRef]
8. Boulogeorgos, A.A.A.; Alexiou, A.; Merkle, T.; Schubert, C.; Elschner, R.; Katsiotis, A.; Rodrigues, F. Terahertz Technologies to Deliver Optical Network Quality of Experience in Wireless Systems Beyond 5G. *IEEE Commun. Mag.* **2018**, *56*, 144–151. [CrossRef]
9. Ndjiongue, A.R.; Ngatched, T.M.N.; Dobre, O.A.; Armada, A.G. VLC-Based Networking: Feasibility and Challenges. *IEEE Netw.* **2020**, *34*, 158–165. [CrossRef]

10. Rao, S.; Digge, J.; Rindhe, B.U. Free Space Optics for 5G and Beyond. In Proceedings of the 2021 6th International Conference for Convergence in Technology (I2CT), Maharashtra, India, 2–4 April 2021; pp. 1–5. [CrossRef]

11. Montero, D.S.; Altuna, R.; López-Cardona, J.D.; Al-Zubaidi, F.M.A.; Vázquez, C. Power-over-Fiber for C-RAN and 6G Networks. In *Advanced Photonics Congress 2023*; Technical Digest Series; Optica Publishing Group: Washington, DC, USA, 2023; p. NeW3B.3.

12. Lei, M.; Li, A.; Hua, B.; Zhang, J.; Cai, Y.; Zou, Y.; Zhu, M. Radar-Assisted MMW-over-Fiber System for B5G Mobile Communications. In *Conference on Lasers and Electro-Optics*; Technical Digest Series; Optica Publishing Group: Washington, DC, USA, 2022; p. SM5J.4.

13. 5G PPP Technology Board. White paper: AI and ML—Enablers for Beyond 5G Networks. 2021, p. 4299895. Available online: https://doi.org/10.5281/zenodo.4299895 (accessed on 14 September 2023).

14. Ghosh, A. Massive MIMO for the New Radio—Overview and Performance. IEEE 5G Summit, June 2017. Available online: http://www.5gsummit.org/hawaii/docs/slides/Amitava-Ghosh.pdf (accessed on 14 September 2023)

15. Abdalla, A.M.; Rodriguez, J.; Elfergani, I.; Teixeira, A. *Optical and Wireless Convergence for 5G Networks*; Wiley-IEEE Press: Hoboken, NJ, USA, 2019; ISBN 9781119491590.

16. United Nations. The 17 Goals. 2020. Available online: https://sdgs.un.org/goals (accessed on 20 September 2023)

17. Hoshida, T.; Curri, V.; Galdino, L.; Neilson, D.T.; Forysiak, W.; Fischer, J.K.; Poggiolini, P. Ultrawideband Systems and Networks: Beyond C + L-Band. *Proc. IEEE* **2022**, *110*, 1725–1741. [CrossRef]

18. Luís, R.S.; Puttnam, B.J.; Rademacher, G.; Klaus, W.; Agrell, E.; Awaji, Y.; Wada, N. On the spectral efficiency limits of crosstalk-limited homogeneous single-mode multi-core fiber systems. In Proceedings of the Advanced Photonics Congress: Photonic Networks and Devices, New Orleans, LO, USA, 24–27 July 2017; p. NeTu2B.2.

19. Sillard, P.; Benyahya, K.; Soma, D.; Labroille, G.; Jian, P.; Igarashi, K.; Shibahara, K. Few-Mode Fiber Technology, Deployments, and Systems. *Proc. IEEE* **2022**, *110*, 1804–1820. [CrossRef]

20. Wu, Q.; Wang, J.; Chen, S.; Kanai, A. Resource allocation problem in multi-band space-division multiplexing elastic optical networks. In Proceedings of the 2022 18th International Conference on Computational Intelligence and Security (CIS), Chengdu, China, 16–18 December 2022; pp. 225–228. [CrossRef]

21. Hosseini, S.; de Miguel, I.; Merayo, N.; Aguado, J.C.; de Dios, Ó.G.; Barroso, R.J.D. Migration of elastic optical networks to the C + L-bands subject to a partial upgrade of the number of erbium-doped fiber amplifiers. *J. Opt. Commun. Netw.* **2023**, *15*, F22–F35. [CrossRef]

22. Nadal, L.; Casellas, R.; Fàbrega, J.M.; Vílchez, F.J.; Moreolo, M.S. Capacity Scaling in Metro-Regional Aggregation Networks: The Multiband S-BVT. *JOCN* **2023**, *15*, F13–F21. [CrossRef]

23. Acacia Communications, Inc. Acacia Introduces Two New 400G QSFP-DD Pluggable Coherent Optical Modules That Further Expand Optical Transceiver Applications, March, 2022. Available online: https://acacia-inc.com/blog/acacia-introduces-two-new-400g-qsfp-dd-pluggable-coherent-optical-modules/ (accessed on 27 September 2023).

24. II-VI Coherent Corp. Coherent Corp 400G ZR+ QSFP-DD-DCO High Tx Output Power Optical Transceiver. 2023. Available online: https://ii-vi.com/product/400g-zr-qsfp-dd-dco-high-tx-output-power-optical-transceiver/ (accessed on 27 September 2023).

25. Zhuge, Q.; Chen, X.; Plant, D.V.; Shieh, W. Feature issue introduction: Ultra-wideband optical communications. *Opt. Express* **2022**, *30*, 13591–13593. [CrossRef]

26. ITU-T G-Series Recommendations—Supplement 39. Optical System Design and Engineering Considerations. 2016. Available online: https://www.itu.int/rec/T-REC-G.Sup39/en (accessed on 25 September 2023)

27. Agrawal, G.P. *Chapter 3 of Nonlinear Fiber Optics*, 5th ed.; Elsevier, Academic Press: Amsterdam, The Netherlands, 2019.

28. Renaudier, J.; Napoli, A.; Ionescu, M.; Calo, C.; Fiol, G.; Mikhailov, V.; Poggiolini, P. Devices and Fibers for Ultrawideband Optical Communications. *Proc. IEEE* **2022**, *110*, 1742–1759. [CrossRef]

29. Napoli, A.; Costa, N.; Fischer, J.K.; ao Pedro, J.; Abrate, S.; Calabretta, N.; Forysiak, W.; Pincemin, E.; Gimenez, J.P.-P.; Matrakidis, C.; et al. Towards multiband optical systems. In Proceedings of the Advanced Photonics Congress 2018, Zurich, Switzerland, 2–5 July 2018; p. NeTu3E.1.

30. Kraemer, R.; Santana, H.; Zhang, S.; Pan B.; Calabretta, N. Lossless SOA-based Multi-band OADM Nodes in Metro Networks. In Proceedings of the OptoElectronics and Communications Conference (OECC) and International Conference on Photonics in Switching and Computing (PSC), Toyama, Japan, 3–6 July 2022. [CrossRef]

31. Saridis, G.M.; Alexandropoulos, D.; Zervas, G.; Simeonidou, D. Survey and Evaluation of Space Division Multiplexing: From Technologies to Optical Networks. *IEEE Commun. Surv. Tutor.* **2015**, *17*, 2136–2156. [CrossRef]

32. Puttnam, B.J.; Rademacher, G.; Luís, R.S. Space-division multiplexing for optical fiber communications. *Optica* **2021**, *8*, 1186–1203. [CrossRef]

33. Sakaguchi, J.; Klaus, W.; Delgado Mendinueta, J.M.; Puttnam, B.J.; Luís, R.S.; Awaji, Y.; Wada, N.; Hayashi, T.; Nakanishi, T.; Watanabe, T.; et al. Realizing a 36-core, 3-mode fiber with 108 spatial channels. In Proceedings of the Optical Fiber Communications Conference, Los Angeles, CA, USA, 22–26 March 2015.

34. Hayashi, T.; Nakanishi, T. Bandwidth density as a figure of merit for few-mode multi-core fibers. *Opt. Express* **2017**, *25*, 24983–24990. [CrossRef]

35. Hayashi, T.; Sakamoto, T.; Yamada, Y.; Ryf, R.; Essiambre, R.J.; Fontaine, N.; Hasegawa, T. Randomly-Coupled Multi-Core Fiber Technology. *Proc. IEEE* **2022**, *110*, 1786–1803. [CrossRef]

36. Gené, J.M.; Winzer, P.J. A universal specification for multicore fiber crosstalk. *IEEE Photon. Technol. Lett.* **2019**, *31*, 673–676. [CrossRef]
37. Puttnam, B.J.; Luís, R.S.; Eriksson, T.A.; Klaus, W.; Delgado, J.-M.; Awaji, Y.; Wada, N. Impact of intercore crosstalk on the transmission distance of QAM formats in multicore fibers. *IEEE Photon. J.* **2016**, *8*, 0601109. [CrossRef]
38. Sambo, N.; Castoldi, P.; D'Errico, A.; Riccardi, E.; Pagano, A.; Moreolo, M.S.; Gimenez, J.P.P. Next generation sliceable bandwidth variable transponders. *IEEE Commun. Mag.* **2015**, *53*, 163–171. [CrossRef]
39. Welch, D.; Napoli, A.; Bäck, J.; Sande, W.; Pedro, J.; Masoud, F.; Wu, K.T. Point-to-Multipoint Optical Networks Using Coherent Digital Subcarriers. *J. Light. Technol.* **2021**, *39*, 5232–5247. [CrossRef]
40. Nadal, L.; Moreolo, M.S.; Fàbrega, J.M.; Casellas, R.; Vílchez, F.J.; Martínez, R.; Muñoz, R. Programmable SDN-enabled S-BVT based on hybrid electro-optical MCM. *J. Opt. Commun. Netw.* **2018**, *10*, 593–602. [CrossRef]
41. Fabrega, J.M.; Vilchez, F.J.; Moreolo, M.S.; Martínez, R.; Quispe, A.; Nadal, L.; Fernández-Palacios, J.P. Experimental demonstration of a metro area network with terabit-capable sliceable bit-rate-variable transceivers using directly modulated VCSELs and coherent detection. *J. Opt. Commun. Netw.* **2023**, *15*, A103–A113. [CrossRef]
42. Moreolo, M.S.; Fabrega, J.M.; Nadal, L.; Martinez, R.; Casellas, R.; Vilchez, J.; Fernandez-Palacios, J.P. Programmable VCSEL-based photonic system architecture for future agile Tb/s metro networks. *J. Opt. Commun. Netw.* **2021**, *13*, A187–A199. [CrossRef]
43. Fontaine, N.K.; Mazur, M.; Ryf, R.; Chen, H.; Dallachiesa, L.; Neilson, D.T. 36-thz bandwidth wavelength selective switch. In Proceedings of the 2021 European Conference on Optical Communication (ECOC), Bordeaux, France, 13–16 September 2021; pp. 1–4.
44. Ye, F.; Tu, J.; Saitoh, K.; Morioka, T. Simple analytical expression for crosstalk estimation in homogeneous trench-assisted multi-core fibers. *Opt. Express* **2014**, *22*, 23007–23018. [CrossRef]
45. *ITU-T G.652*; Characteristics of a Single-Mode Optical Fibre and Cable. International Telecommunication Union: Geneva, Switzerland, 2017.
46. Nadal, L.; Moreolo, M.S.; Hernández, J.A.; Fabrega, J.M.; Casellas, R.; Muñoz, R.; Martínez, R. SDN-Enabled S-BVT for Disaggregated Networks: Design, Implementation and Cost Analysis. *J. Light. Technol.* **2020**, *38*, 3037–3043. [CrossRef]